# Analytical Modeling of Axial Air Gap Solid Rotor Induction Machines Using a Quasi-Three-Dimensional Method

Mehran Mirzaei[1], Mojtaba Mirsalim[2], and Seyed Ehsan Abdollahi[2]

[1]Electrical Machines and Transformer Research Laboratory, Amirkabir University of Technology, Tehran, Iran
[2]Electrical Engineering Department, Amirkabir University of Technology, Tehran, Iran

**This paper presents an analytical model of axial air gap induction motors with solid rotors that includes the two-dimensional current distribution in the rotor. The model is quasi-three-dimensional and considers the circumferential as well as radial and angular dimensions. Also, one can consider the various arrangements of the stator windings i.e., single layer, double layer, and gramme for this type of motor. The method is valid for both constant current and constant voltage sources. Comparison of the simulation results of the produced torque with the experimental ones shows the high accuracy of the proposed method.**

***Index Terms*—Analytical, axial air gap, induction machine, solid rotor.**

## I. Introduction

THE induction motor with an axial air gap and a flat homogenous disk rotor shows some performance characteristics that are superior to conventional induction machines. An axial air gap type induction machine promises high utilization of the active materials and thus favorable power density [1]. High rotational speeds and small moment of inertia of the motor promise high power densities and small mechanical time constants and make it a suitable choice for servo and high-speed applications.

A complete analysis is required for the exact performance estimation of axial air gap induction motors. Many papers have been published in the literature about the analysis of axial air gap induction motors with solid rotors that include numerical and analytical methods [2]–[11]. One can deduce from the papers that the results are not sufficiently accurate and give rise to errors in machine performance estimations.

Here, a method with a high degree of accuracy for the prediction of electromagnetic fields is presented. The computational treatment is based on the solution of field equations written in cylindrical coordinates. The analytical approach described herein leads to a mathematical model, which is also a practical design tool. For accuracy evaluation of the proposed method, the computed results are compared with experimental data and three-dimensional finite-element method (3-D FEM).

## II. Modeling

As it is shown in Fig. 1, axial air gap induction motors come in a variety of structures. Fig. 1(a) depicts a single-sided motor with a solid iron rotor; while a double-layer aluminum- solid iron rotor type is shown in Fig. 1(b). In Fig. 1(c), one can observe the schematic of a double-sided motor with a solid aluminum or iron rotor.

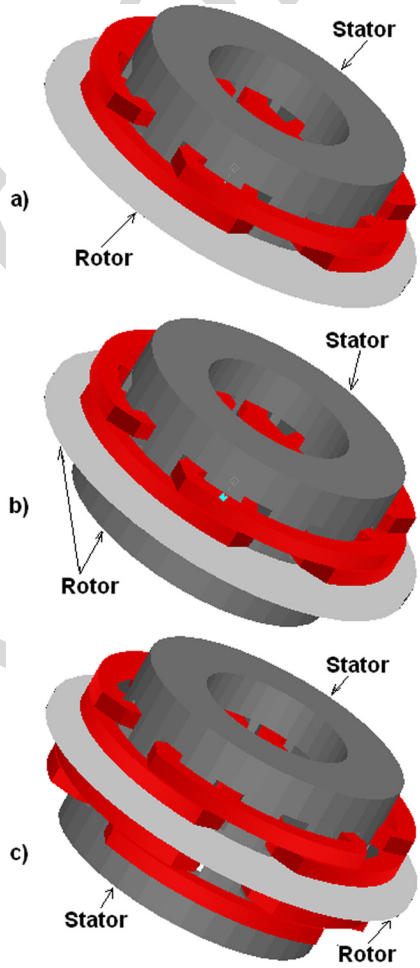


Fig. 1. Different configurations of axial air-gap induction motors.

### A. Mathematical Modeling

The computation coordinates are depicted in Figs. 2 and 3. In electrical machines, the 3-D air-gap magnetic flux has two parts:

1) the one that reaches the rotor surface (the effective part);
2) the total leakage flux (including stator winding leakage flux).

Digital Object Identifier 10.1109/TMAG.2007.894215

Color versions of one or more of the figures in this paper are available online at http://ieeexplore.ieee.org.

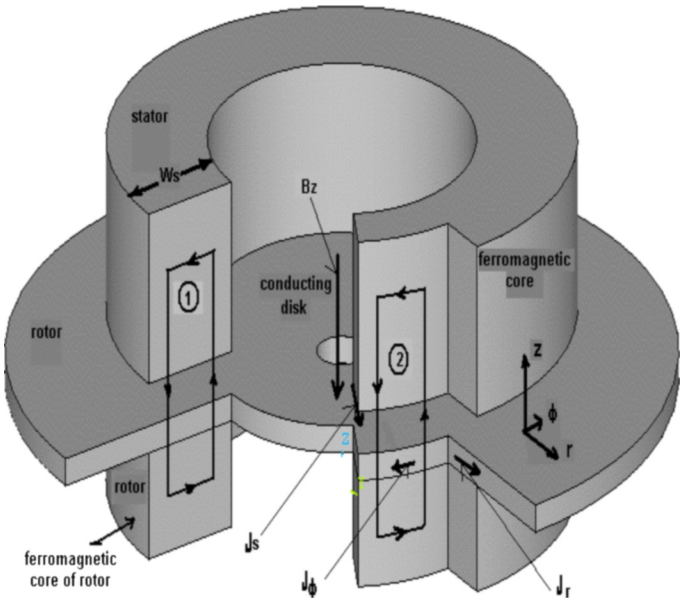


Fig. 2. 3-D view of the mathematical model.

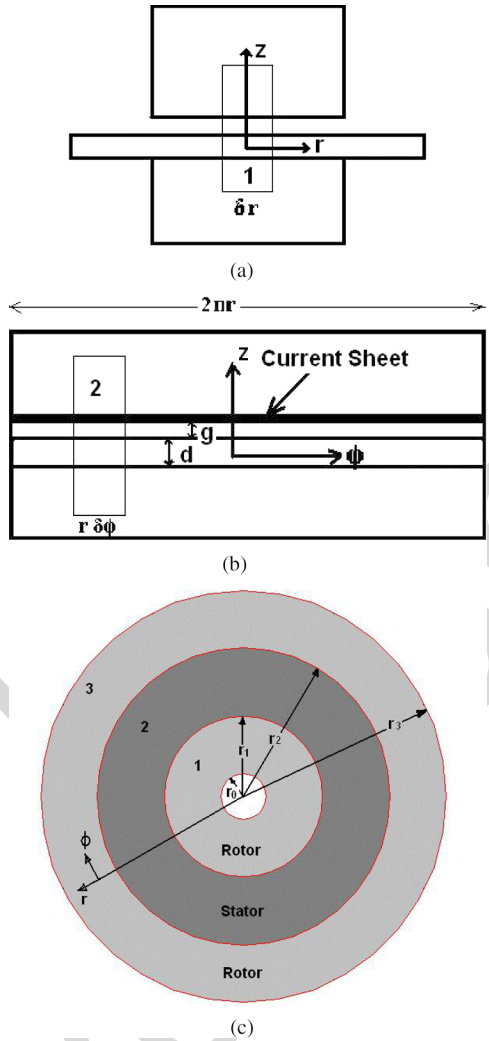


Fig. 3. Two-dimensional views: (a) r-z view, (b) z-$\phi$ view, and (c) r-$\phi$ view.

The following assumptions are made for the modeling [13].

1) Only the axial component of the flux density, $Bz$ is considered (because this component is more effective).
2) The variation of field intensity and currents along the z-axis are zero [10].
3) The mutual flux is normal to the rotor surface.
4) The relative permeability of rotor and stator ferromagnetic parts is considered to be very high $(\infty)$.

The proposed method can be applied to both single-sided and double-sided disk motors. By applying the Ampere's law to the two elementary loops (1, 2) in Fig. 3(a) and (b), the following equations are obtained [12], [13]:

$$\frac{gt}{\mu 0}\frac{\partial Bz}{r\partial\phi} = Js + Jr2 \tag{1}$$

$$-\frac{gt}{\mu 0}\frac{\partial Bz}{\partial r} = J\phi 2. \tag{2}$$

Here, $g_t$ is the total distance between the two ferromagnetic parts of rotor and stator [air-gap (g) plus the nonferromagnetic conducting part of the rotor (d)] and $\mu_0$ is the air magnetic permeability. According to Fig. 3(c), $J_{r2}$ and $J_{\Phi 2}$ are two components of current density in region (2) below the stator core. Now, consider a symmetric time-harmonic current system, where the three phases are arbitrary star connected. The resulting equivalent surface current density distribution from stator winding is as follows [14]:

$$Js = \frac{4N}{j2\pi r}2^{0.5}I_1\sum_{v}^{\pm\infty}{}^{v}k_w \exp j(\omega t - v'\phi)$$

$$v = +1, -5, +7, -11, +13, \ldots, v' = pv$$

$${}^{v}k_w = {}^{v}k'_w \cdot {}^{v}k''_w \cdot {}^{v}k'''_w$$

$${}^{v}k'_w = 0.5\frac{\sin(pmqv'\alpha)}{\sin(0.5(v'mq\alpha - \pi))}\frac{\sin(0.5v'q\alpha)}{\sin(0.5v'\alpha)}$$

$${}^{v}k''_w = \sin\left(v'\frac{mq-\varepsilon}{2}\alpha\right)\frac{\sin(0.5(v'mq\alpha - \pi))}{\sin(0.5(v'q\alpha - \pi/m))}$$

$${}^{v}k'''_w = \frac{\sin\left(0.5\frac{sw}{sp}v'\alpha\right)}{0.5\frac{sw}{sp}v'\alpha}, \quad \alpha = \frac{2\pi}{2pmq} \tag{3}$$

where $N, \omega$, and $I_1$ are number of turns in each coil, the angular supply frequency, and phase current, respectively. $sw, sp, m, p, q$, and $\varepsilon$ are respectively the stator slot opening, the slot pitch, number of phases, pole pairs, number of slots per pole per phase, and the reduction in width of coils in the units of slots. All magnetic and electric fields are a function of $\exp j(\omega t - v'\phi)$.

When Ohm's law is applied to a loop lying in $r$-$\phi$ plane, the following relation is obtained:

$$\frac{\rho_s}{r}\left(\frac{\partial}{\partial r}(rJ\phi 2) - \frac{\partial}{\partial\phi}(Jr2)\right) = -\frac{\partial Bz}{\partial t} - \omega\frac{\partial Bz}{\partial\phi}$$

$$\rho_s = \frac{\rho}{d} \tag{4}$$

where $\rho$ is the resistance coefficient of the rotor and $\omega$ is the angular frequency.

From (1)–(2) and (4), (5) is obtained:

$$r^2\frac{\partial^2 Bz}{\partial r^2}+r\frac{\partial Bz}{\partial r}-v'^2Bz+j\left(v'\frac{1}{p}(1-s)-1\right)\omega.$$
$$Kr^2Bz+\frac{\mu 0}{gt}jv'\cdot r\cdot Jsm=0 \quad K=\frac{\mu 0}{\rho_s gt}$$
$$J_{sm}=\frac{4N}{j2\pi r}2^{0.5}{I_1}^v k_w. \tag{5}$$

Because the magnetic flux densities in regions 1 and 3 (out of the stator ferromagnetic regions) are negligible, current fields are Laplacian as follows [12], [13]:

$$\begin{aligned}
&\nabla^2 Jr1=0 \quad , \quad \nabla^2 Jr3=0\\
&\nabla^2 J\phi 1=0 \quad , \quad \nabla^2 J\phi 3=0\\
&r^2\frac{\partial^2 Jr1}{\partial r^2}+3r\frac{\partial Jr1}{\partial r}+(1-v'^2)Jr1=0\\
&r^2\frac{\partial^2 Jr3}{\partial r^2}+3r\frac{\partial Jr3}{\partial r}+(1-v'^2)Jr3=0\\
&r^2\frac{\partial^2 J\phi 1}{\partial r^2}+3r\frac{\partial J\phi 1}{\partial r}+(1-v'^2)J\phi 1=0\\
&r^2\frac{\partial^2 J\phi 3}{\partial r^2}+3r\frac{\partial J\phi 3}{\partial r}+(1-v'^2)J\phi 3=0.
\end{aligned} \tag{6}$$

The subscripts 1 and 3 refer to regions 1 and 3. The assumptions and simplifications made to obtain and solve the equations have completely been discussed in [13].

### B. Solutions

The solutions to (6) in regions 1 and 3 are

$$\begin{aligned}
Jr1&=C11\cdot r^{(-v'-1)}+C12\cdot r^{(v'-1)}\\
Jr3&=C31\cdot r^{(-v'-1)}+C32\cdot r^{(v'-1)}\\
J\phi 1&=j(C11\cdot r^{(-v'-1)}-C12\cdot r^{(v'-1)})\\
J\phi 3&=j(C31\cdot r^{(-v'-1)}-C32\cdot r^{(v'-1)})
\end{aligned} \tag{7}$$

where $C11, C12, C31$, and $C32$ are constants that can be obtained using the related boundary conditions.

Equation (5) is not easily solved, and in order to get a solution in the region under the stator [region (2)], two methods are presented.

*1) Method One:* The resultant field equations are solved analytically in Maple environment [15]. The particular solutions depend on the number of poles. Equation (5) has both a particular and a general answer. The particular solution depends on whether the number of pole pairs is odd or even, but the general solution remains unchanged.

If the number of pole pairs is odd, then

$$\begin{aligned}
Bz=&\,C21\cdot Besselk(v',j(jA)^{0.5}r)\\
&+C22\cdot Besselj(v',(jA)^{0.5}r)\\
&-B\cdot LommelS1(-1,v',(A)^{0.5}r)\\
j=\sqrt{-1},&\quad A=\left(v'\frac{2}{P}(1-s)-1\right)\cdot K\cdot\omega\\
B=\frac{\mu 0}{gt}v'\cdot r\cdot J'sm,&\quad J'sm=\frac{Jsm}{r}
\end{aligned} \tag{8}$$

where $LommelS1$, $Besselj$, and $Besselk$ are mathematical functions [15].

On the other hand, if the number of pole pairs is even, the solutions depend on harmonic order and the number of pole pairs. As an example, the fundamental component of $Bz$ for a four-pole motor is

$$\begin{aligned}
Bz=&\,C21\cdot Besselk(v',j(jA)^{0.5}r)\\
&+C22\cdot Besselj(v',(jA)^{0.5}r)-\frac{B}{Ar^2}.
\end{aligned} \tag{9}$$

The constants in (7), (8), and (9) are calculated from the boundary conditions in the region numbers (1)–(2) and (3). The boundary conditions are

$$\begin{aligned}
&Jr1(r=r0)=0\\
&Jr3(r=r3)=0\\
&Jr2(r=r1)=Jr1(r=r1)\\
&Jr2(r=r2)=Jr3(r=r2)\\
&J\phi 1(r=r1)=J\phi 2(r=r1)\\
&J\phi 2(r=r2)=J\phi 3(r=r2)
\end{aligned} \tag{10}$$

where $(r0, r3)$ and $(r1, r2)$ are respectively the inner and outer radii of the rotor and stator.

*2) Method Two:* To solve (5), the region under the stator [region (2)] is divided into many concentric circular areas as shown in Fig. 4. The coefficients ($r^2$ and $r$) in the first and second terms of (5) are assumed constant in each circular area. Hence, the equation is converted into a simple second-order equation. Now, the solution in each area is obtained as in the following:

$$\begin{aligned}
Bz(i)=&\frac{-jB}{jA-v'^2}+C21(i)\cdot\exp(\alpha_1(i)\cdot r)\\
&+C22(i)\cdot\exp(\alpha_2(i)\cdot r)\\
\alpha_1(i)=&\frac{-\frac{1}{r2'(i)}+\sqrt{\left(\frac{1}{r2'(i)}\right)^2-4\left(jA-\frac{v'^2}{r2'(i)^2}\right)}}{2}\\
\alpha_2(i)=&\frac{-\frac{1}{r2'(i)}-\sqrt{\left(\frac{1}{r2'(i)}\right)^2-4\left(jA-\frac{v'^2}{r2'(i)^2}\right)}}{2}\\
r2'(i)=&\,r1+\frac{(r2-r1)}{n}\cdot\frac{(2i-1)}{2}
\end{aligned} \tag{11}$$

where $n$ is the number of areas and $i$ is the area number.

The constants in (7) and (11) are calculated from the boundary conditions in the region numbers (1)–(2) and (3) as before. The boundary conditions are

$$\begin{aligned}
&Jr1|_{(r=r0)}=0\\
&Jr3|_{(r=r3)}=0\\
&Jr2(i=1)|_{(r=r1)}=Jr1|_{(r=r1)}\\
&J\phi 2(i=1)|_{(r=r1)}=J\phi 1|_{(r=r1)}\\
&\vdots\\
&Jr2(i)|_{(r=r2(i))}=Jr2(i+1)|_{(r=r2(i))}\\
&J\phi 2(i)|_{(r=r2(i))}=J\phi 2(i+1)|_{(r=r2(i))}\\
&\vdots
\end{aligned}$$

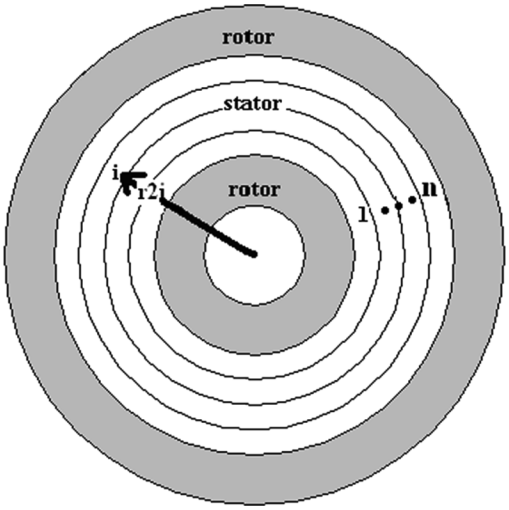


Fig. 4. Concentric circular areas of region (2).

$$Jr2(i=n)|_{(r=r2)} = Jr3|_{(r=r2)}$$
$$J\phi 2(i=n)|_{(r=r2)} = J\phi 3|_{(r=r2)}$$
$$\vdots$$
$$r2(i) = r1 + i\frac{(r2-r1)}{n}. \tag{12}$$

## III. Simulation

To evaluate the accuracy of the analytical model, an axial air gap induction motor with considerable space harmonics is selected. The motor has four poles, three phases, and 12 slots. Other specifications are in Table I. In order for the effects of harmonics to be high, one slot per pole per phase is chosen. The orders of the important existing harmonics are $1, -5, 7$, and $-11$, while the effects of the others are negligible. First, the solutions from method one is presented:

$$\begin{aligned}
Bz,1 &= C21,1 \cdot Besselk(2, j(jA)^{0.5}r) \\
&\quad + C22,1 \cdot Besselj(2,(jA)^{0.5}r) \\
&\quad - BAr^{-2} \\
Bz,-5 &= C21,-5 \cdot Besselk(10, j(jA)^{0.5}r) \\
&\quad + C22,-5 \cdot Besselj(10,(jA)^{0.5}r) \\
&\quad - B(18579456 \\
&\quad + 516096jAr^2 - 8064.A^2r^4 - 96jA^3r^6 \\
&\quad + A^4r^8) * A^{-5}r^{-10} \\
Bz,7 &= C21,7 \cdot Besselk(14, j(jA)^{0.5}r) \\
&\quad + C22,7 \cdot Besselj(14,(jA)^{0.5}r) \\
&\quad - B(-3643696742\,400 \\
&\quad - 7007109120\,0jAr^2 729907200A^2r^4 \\
&\quad + 5529600jA^3r^6 - 34560A^4r^8 \\
&\quad - 192jA^5r^{10} + A^6r^{12}) * A^{-7}r^{-14} \\
Bz,-11 &= C21,-11 \cdot Besselk(22, j(jA)^{0.5}r) \\
&\quad + C22,-11 \cdot Besselj(22,(jA)^{0.5}r) \\
&\quad - B(-4870248707\,1493088870\,40000 \\
&\quad - 5797915127\,5587010560\,000jAr^2 \\
&\quad \times 3623696954\,7241881600\,0 * A^2r^4 \\
&\quad \times 1589340769\,615872000jA^3r^6 \\
&\quad - 5518544338\,944000A^4r^8 \\
&\quad - 1623101276\,1600jA^5r^{10} \\
&\quad + 42268262400A^6r^{12} \\
&\quad + 100638720jA^7r^{14} \\
&\quad - 224640A^8r^{16} - 480jA^9r^{18} \\
&\quad + \mathrm{A}^{10}\mathrm{r}^{20}) * A^{-11}r^{-22}.
\end{aligned}$$

TABLE I
Design Data of the Machine (All Length Dimensions in Millimeters)

| Parameter | Value |
|---|---|
| $p$ | 2 |
| $q$ | 1 |
| $m$ | 3 |
| Stator inner diameter | 71 |
| Stator outer diameter | 128 |
| Rotor inner diameter(Al) | 15 |
| Rotor outer diameter(Al) | 184 |
| Rotor inner diameter(Fe) | 71 |
| Rotor outer diameter(Fe) | 128 |
| Rotor (Al) conductivity(S/m) | 3.278e7 |
| Relative Magnetic Permeability of Stator and Rotor Iron | 250 |
| Number of Stator Slots | 12 |
| Stator Height | 39 |
| Number of Turns per Coil | 290 |
| Stator Slot Opening | 3 |
| Stator Slot Width | 14 |
| Stator to Rotor Clearance | 1 |
| Rotor (Fe) Thickness | 25 |
| Rotor (Al) Thickness | 6.35 |
| Slot Height | 21 |
| Frequency | 50 |
| Current($I_l$) | 2 (A) |

As it can be seen, the solutions for the high harmonics are very complex and hard to solve.

The machine torque is obtained from the following equation:

$$\begin{aligned}
\text{Torque} &= \pi \cdot r_{\text{mean}} \cdot (r2-r1) \\
&\quad \cdot \text{real}(Bz(r_{\text{mean}}) \cdot \text{conjugate}(J'sm)) \\
r_{\text{mean}} &= \frac{(r2+r1)}{2}.
\end{aligned} \tag{13}$$

To consider the effect of the magnetic flux of the winding overhangs and the related leakage fluxes, the width of stator core$(r2-r1)$ should be increased from 0.5 gt to 2 gt [10].

In using method two for simulation, the number $n = 21$ is found to give sufficient accuracy. The machine torque is obtained from the following equation:

$$\begin{aligned}
\text{Torque} &= \sum_{i=1}^{n} \pi \cdot r2'(i) \\
&\quad \cdot \text{real}(Bz(r2'(i)) \cdot \text{Conjugate}(J'sm) \cdot \Delta r \\
\Delta r &= \frac{r2-r1}{n}.
\end{aligned} \tag{14}$$

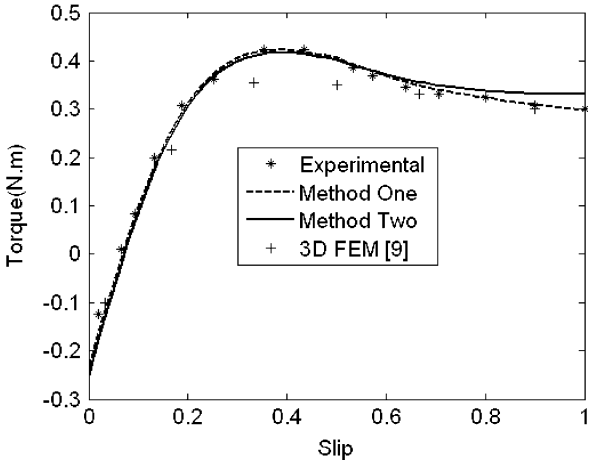


Fig. 5. Comparison of the predicted torque with the experimental one and 3-D FEM results [9].

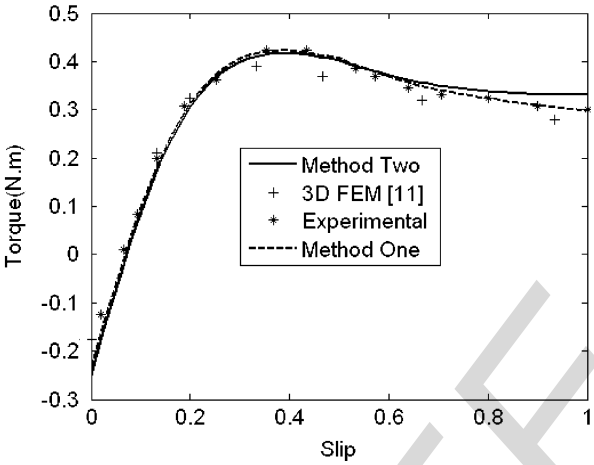


Fig. 6. Comparison of the predicted torque with the experimental one and 3-D FEM results [11].

Now, the results are compared with the experimental ones [9], [10] and depicted in Fig. 5. The calculated results coincide very well with the experimental ones. It is observed that the results of the presented method have higher accuracy in comparison with the 3-D FEM [9], [10]. The authors believe that one of the error sources of the 3-D FEM at low slips might be because of the chosen low mesh density (73 224 elements). Also in [11], the machine has been analyzed using 3-D FEM (882 561 elements). In [9], a stationary mesh has been used, and velocity and rotor motion effects have been directly employed in formulations. But in [11], a moving mesh has been applied. The results of [11] are compared with the obtained analytical ones in Fig. 6. The errors in [9] and [11] are considerable.

The obtained results of method one are better than method two, because an exact solution of field equations has been used.

The plots of computed magnetic flux density along with 3-D FEM results are shown in Figs. 7 and 8.

The 3-D FEM analysis has been carried out by OPERA-3D software with ELEKTRA module [16]. Comparison between analytical and 3-D FEM shows the accuracy of the proposed method in magnetic field calculations of axial air-gap in induction machines. The oscillations in 3-D FEM results of Fig. 8 are due to the teeth and slot effects.

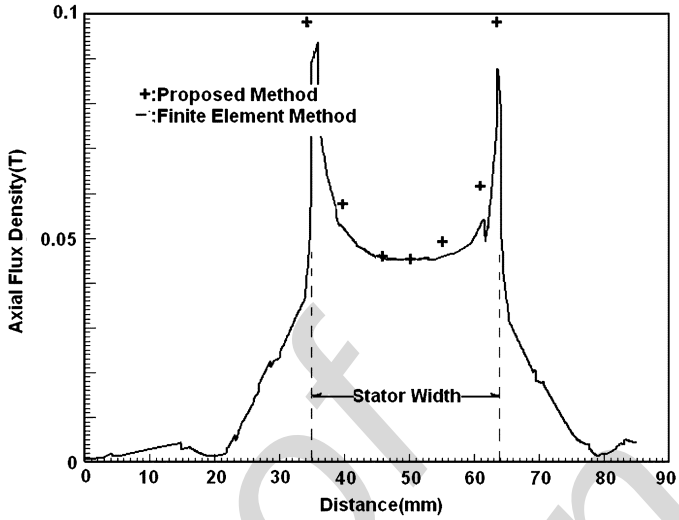


Fig. 7. Comparison between analytical and 3-D FEM in radial direction.

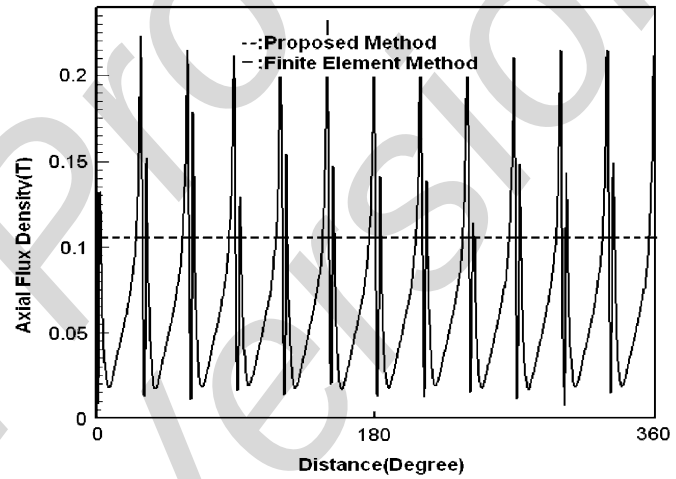


Fig. 8. Comparison between analytical and 3-D FEM in angular direction under the stator, in middle of the air gap and mean radius of the stator.

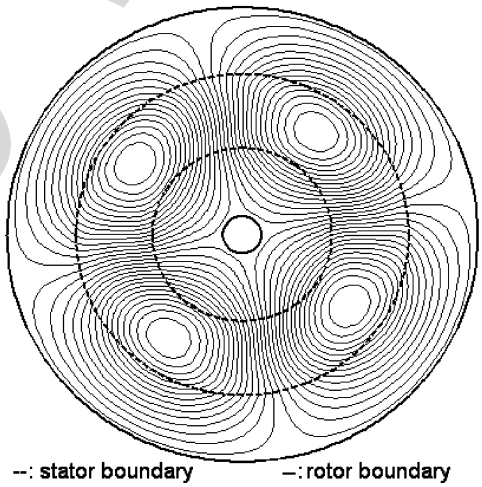


Fig. 9. Rotor current density distribution at zero speed.

The rotor current distribution at zero speed is shown in Fig. 9. One can deduce from the distribution that three-dimensional analysis is necessary for complete consideration of machine structure and exact prediction of its performance.

## IV. Conclusion

A direct solution of the field equations in cylindrical coordinates has been presented. The analytical method considers almost all dimensions of the machine. At low slips (normal operating region), the predicted points of both methods coincide with the experimental results with high accuracy. Hence, the proposed method has the ability of accurate performance prediction of axial air gap solid rotor induction machines. The presented approach helps designers to compute and evaluate performances of axial air gap induction machines with solid rotors in shorter time and with high accuracy.

**AUTHOR: The editor-in-chief requests that you please add two or more references to your paper citing recent *IEEE Transactions on Magnetics* articles (published in 2005-2007), to demonstrate that your paper is relevant to current interests of our audience. Please let me know if you are able to do this. Thank you. —Ed.**

## References

[1] S. Kubzdela and B. Weglinski, "Magnetodielectrics in induction motors with disk rotor," *IEEE Trans. Magn.*, vol. 24, no. 1, pp. 635–638, Jan. 1988.
[2] I. Boldea and S. A. Nasar, "Finite width, finite thickness and saturation effects in solid-rotor induction machines," *IEEE Trans. Power App. Syst.*, vol. 94, no. 5, pp. 1500–1507, Sep. 1975.
[3] H. May, "Analysis, performance and equivalent circuit of a disk-rotor induction machine," (in German) *ETZ A*, vol. 104, no. 10, pp. 574–577, 1973.
[4] H. Mosebach, "Analysis and characteristics of the disk-rotor induction machine," *Elect. Mach. Electromech.*, vol. 1, pp. 87–98, 1976.
[5] N. Esposito, A. Musolino, and B. Tellini, "Electromagnetic analysis of an induction motor with massive disk," *IEEE Trans. Magn.*, vol. 31, no. 3, pp. 2076–2079, May 1995.
[6] K. Ciosk, E. Gierczak, and E. Mendrela, "Analysis of electromagnetic field in a disk induction motor with double-sided stator and twin rotors using a 3-D reluctance network method," in *ICEM. 98*, Istanbul, Turkey, 1998, pp. 286–289.
[7] E. Mendrela, "Evaluation of magnetic field and forces in a single-phase induction disk motor with multi-layer rotor," *Arch. Elect. Eng.*, vol. XLIV, no. 2, pp. 263–273, 1996.
[8] A. I. Inkin and B. V. Litvinov, "The electromagnetic field in the gap of A.C. faceplate motors," *Elektrichestvo*, no. 11, pp. 67–71, 1974.
[9] D. Rodger, P. C. Coles, N. Allen, H. C. Lai, P. J. Leonard, and P. Roberts, "3D finite element model of a disc induction machine," in *IEE 8th Int. Conf. Electrical Machines and Drives (EMD97)*, 1997, pp. 148–149.
[10] D. Rodger, H. C. Lai, P. C. Coles, and R. J. Hill-Cottingham, "Modeling axial air gap induction machine," in *IEE Seminar Axial Air Gap Machines*, 2001, pp. 2/1–2/3.
[11] D. N. Dyck, B. Forghani, C. S. Brett, J. P. Webb, and D. A. Lowther, "A T-omega finite element method for arbitrary motion in 3D," presented at the Compumag 2005, Shenyang, China.
[12] S. A. Nasar and I. Boldea, *Linear Motion Electric Machines*. New York: Wiley, 1976.
[13] C. H. Lee and C. Y. Chin, "A theoretical analysis of linear induction motors," *IEEE Trans. Power App. Syst.*, vol. 98, no. 2, pp. 679–688, Mar. 1979.
[14] K. Oberretl, "Three-dimensional analysis of the linear motor," in *Transport Without Wheels*. London, U.K.: Elek Science, 1977, pp. 217–247.
[15] Maple ver. 7, Software User Guide. 2001.
[16] Pc-Opera ver.8.5, Software User Guide. 2002.

Manuscript received September 22, 2006; revised February 23, 2007. Corresponding author: M. Mirzaei (e-mail: mehranamirzaei@yahoo.com).

**Mehran Mirzaei** was born in Bandar Anzali, Iran, in 1977. He received the B.S. and M.S. degrees in electrical power engineering from Amirkabir University of Technology, Tehran, Iran, in 1999 and 2002, respectively.

Currently, he is with the EMTR Laboratory, Amirkabir University of Technology. His research interests are numerical and analytical analysis of electromagnetic fields, solid rotor and linear induction machines, and high-speed electric machines.

**Mojtaba Mirsalim** (SM'04) was born in Tehran, Iran, on February 14, 1956. He received the B.S. degree in EECS/NE and the M.S. degree in nuclear engineering from the University of California, Berkeley, in 1978 and 1980, respectively, and the Ph.D. degree in electrical engineering from Oregon State University, Corvallis, in 1986.

Since 1987, he has been at Amirkabir University of Technology, Tehran, where he has served five years as the Vice Chairman and more than seven years as the General Director in Charge of Academic Assessments, and currently is a Full Professor in the department of Electrical Engineering where he teaches courses and conducts research in energy conversion, electrical machine design, and hybrid vehicles, among others. His special fields of interest include the design, analysis, and optimization of electric machines, FEM, renewable energy and hybrid vehicles. He is the author of more than 90 international journal and conference papers and three books on electric machinery and FEM. He is the founder and at present, the director of the Electrical Machines & Transformers Research Laboratory (http://ele.aut.ac.ir/EMTRL/Homepage.htm).

**Seyed Ehsan Abdollahi** received the B.Sc. degree from Amirkabir University of Technology (Tehran Polytechnic), Tehran, Iran, with 1st rank of honor in 2002 and the M.S. degree from Iran University of Science & Technology, Tehran, in 2005, both in electrical engineering.

Currently, he is with the EMTR Laboratory, Amirkabir University of Technology. His current research interests are electric machine design and analysis including analytical and numerical methods and also modeling of microturbine generation systems.

# Analytical Modeling of Axial Air Gap Solid Rotor Induction Machines Using a Quasi-Three-Dimensional Method

Mehran Mirzaei[1], Mojtaba Mirsalim[2], and Seyed Ehsan Abdollahi[2]

[1]Electrical Machines and Transformer Research Laboratory, Amirkabir University of Technology, Tehran, Iran
[2]Electrical Engineering Department, Amirkabir University of Technology, Tehran, Iran

**This paper presents an analytical model of axial air gap induction motors with solid rotors that includes the two-dimensional current distribution in the rotor. The model is quasi-three-dimensional and considers the circumferential as well as radial and angular dimensions. Also, one can consider the various arrangements of the stator windings i.e., single layer, double layer, and gramme for this type of motor. The method is valid for both constant current and constant voltage sources. Comparison of the simulation results of the produced torque with the experimental ones shows the high accuracy of the proposed method.**

*Index Terms*—**Analytical, axial air gap, induction machine, solid rotor.**

## I. Introduction

THE induction motor with an axial air gap and a flat homogenous disk rotor shows some performance characteristics that are superior to conventional induction machines. An axial air gap type induction machine promises high utilization of the active materials and thus favorable power density [1]. High rotational speeds and small moment of inertia of the motor promise high power densities and small mechanical time constants and make it a suitable choice for servo and high-speed applications.

A complete analysis is required for the exact performance estimation of axial air gap induction motors. Many papers have been published in the literature about the analysis of axial air gap induction motors with solid rotors that include numerical and analytical methods [2]–[11]. One can deduce from the papers that the results are not sufficiently accurate and give rise to errors in machine performance estimations.

Here, a method with a high degree of accuracy for the prediction of electromagnetic fields is presented. The computational treatment is based on the solution of field equations written in cylindrical coordinates. The analytical approach described herein leads to a mathematical model, which is also a practical design tool. For accuracy evaluation of the proposed method, the computed results are compared with experimental data and three-dimensional finite-element method (3-D FEM).

## II. Modeling

As it is shown in Fig. 1, axial air gap induction motors come in a variety of structures. Fig. 1(a) depicts a single-sided motor with a solid iron rotor; while a double-layer aluminum- solid iron rotor type is shown in Fig. 1(b). In Fig. 1(c), one can observe the schematic of a double-sided motor with a solid aluminum or iron rotor.

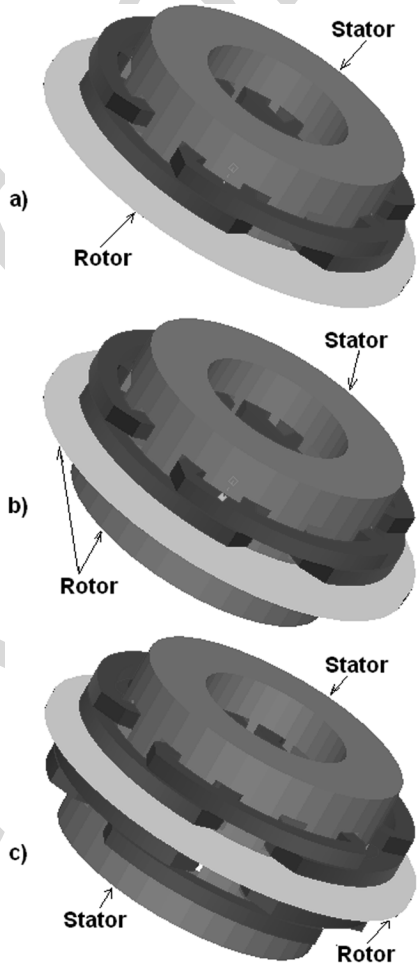


Fig. 1. Different configurations of axial air-gap induction motors.

### A. Mathematical Modeling

The computation coordinates are depicted in Figs. 2 and 3. In electrical machines, the 3-D air-gap magnetic flux has two parts:

1) the one that reaches the rotor surface (the effective part);
2) the total leakage flux (including stator winding leakage flux).

Digital Object Identifier 10.1109/TMAG.2007.894215

Color versions of one or more of the figures in this paper are available online at http://ieeexplore.ieee.org.

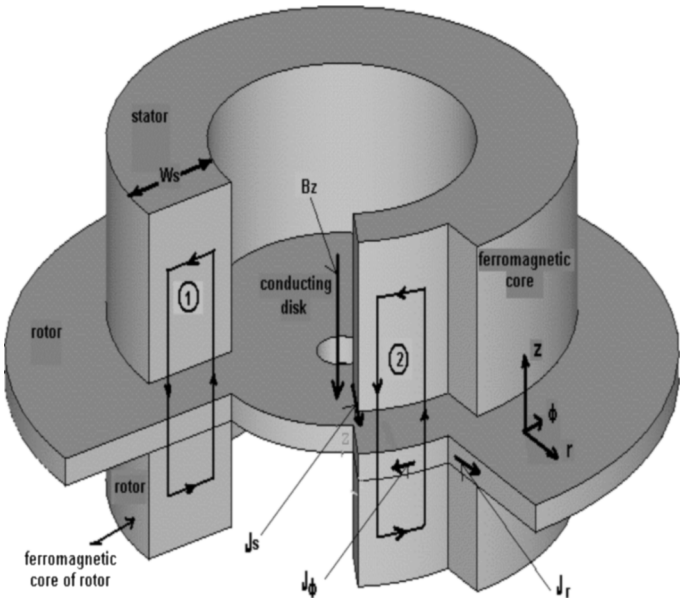


Fig. 2. 3-D view of the mathematical model.

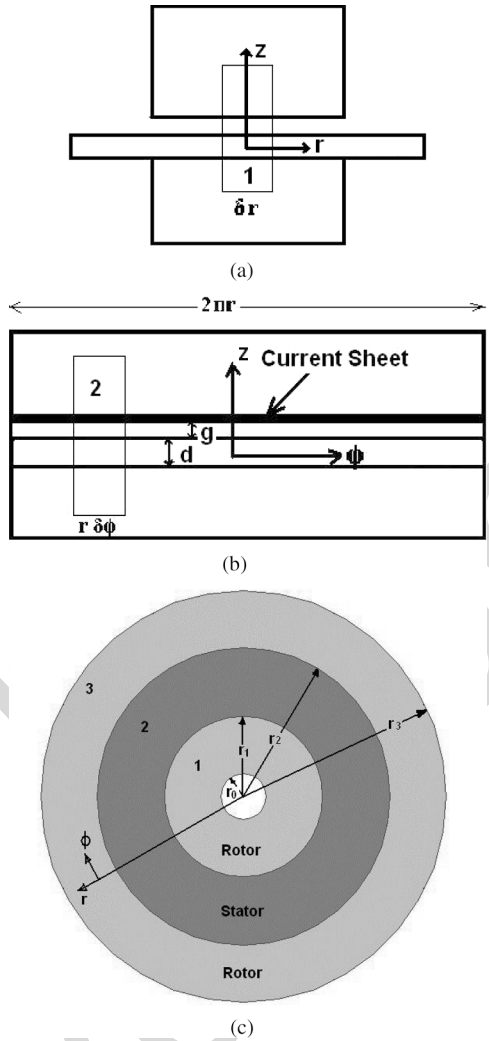


Fig. 3. Two-dimensional views: (a) r-z view, (b) z-$\phi$ view, and (c) r-$\phi$ view.

The following assumptions are made for the modeling [13].

1) Only the axial component of the flux density, $Bz$ is considered (because this component is more effective).
2) The variation of field intensity and currents along the z-axis are zero [10].
3) The mutual flux is normal to the rotor surface.
4) The relative permeability of rotor and stator ferromagnetic parts is considered to be very high $(\infty)$.

The proposed method can be applied to both single-sided and double-sided disk motors. By applying the Ampere's law to the two elementary loops (1, 2) in Fig. 3(a) and (b), the following equations are obtained [12], [13]:

$$\frac{gt}{\mu 0}\frac{\partial Bz}{r\partial\phi} = Js + Jr2 \tag{1}$$

$$-\frac{gt}{\mu 0}\frac{\partial Bz}{\partial r} = J\phi 2. \tag{2}$$

Here, $g_t$ is the total distance between the two ferromagnetic parts of rotor and stator [air-gap (g) plus the nonferromagnetic conducting part of the rotor (d)] and $\mu_0$ is the air magnetic permeability. According to Fig. 3(c), $J_{r2}$ and $J_{\Phi 2}$ are two components of current density in region (2) below the stator core. Now, consider a symmetric time-harmonic current system, where the three phases are arbitrary star connected. The resulting equivalent surface current density distribution from stator winding is as follows [14]:

$$Js = \frac{4N}{j2\pi r}2^{0.5}I_1\sum_{v}^{\pm\infty}{}^{v}k_w \exp j(\omega t - v'\phi)$$

$$v = +1, -5, +7, -11, +13, \ldots, v' = pv$$

$${}^{v}k_w = {}^{v}k'_w \cdot {}^{v}k''_w \cdot {}^{v}k'''_w$$

$${}^{v}k'_w = 0.5\frac{\sin(pmqv'\alpha)}{\sin(0.5(v'mq\alpha - \pi))}\frac{\sin(0.5v'q\alpha)}{\sin(0.5v'\alpha)}$$

$${}^{v}k''_w = \sin\left(v'\frac{mq-\varepsilon}{2}\alpha\right)\frac{\sin(0.5(v'mq\alpha - \pi))}{\sin(0.5(v'q\alpha - \pi/m))}$$

$${}^{v}k'''_w = \frac{\sin\left(0.5\frac{sw}{sp}v'\alpha\right)}{0.5\frac{sw}{sp}v'\alpha}, \quad \alpha = \frac{2\pi}{2pmq} \tag{3}$$

where $N, \omega$, and $I_1$ are number of turns in each coil, the angular supply frequency, and phase current, respectively. $sw, sp, m, p, q$, and $\varepsilon$ are respectively the stator slot opening, the slot pitch, number of phases, pole pairs, number of slots per pole per phase, and the reduction in width of coils in the units of slots. All magnetic and electric fields are a function of $\exp j(\omega t - v'\phi)$.

When Ohm's law is applied to a loop lying in $r$-$\phi$ plane, the following relation is obtained:

$$\frac{\rho_s}{r}\left(\frac{\partial}{\partial r}(rJ\phi 2) - \frac{\partial}{\partial\phi}(Jr2)\right) = -\frac{\partial Bz}{\partial t} - \omega\frac{\partial Bz}{\partial\phi}$$

$$\rho_s = \frac{\rho}{d} \tag{4}$$

where $\rho$ is the resistance coefficient of the rotor and $\omega$ is the angular frequency.

From (1)–(2) and (4), (5) is obtained:

$$r^2\frac{\partial^2 Bz}{\partial r^2}+r\frac{\partial Bz}{\partial r}-v'^2Bz+j\left(v'\frac{1}{p}(1-s)-1\right)\omega.$$
$$Kr^2Bz+\frac{\mu 0}{gt}jv'\cdot r\cdot Jsm=0 \quad K=\frac{\mu 0}{\rho_s gt}$$
$$J_{sm}=\frac{4N}{j2\pi r}2^{0.5}{I_1}^v k_w. \tag{5}$$

Because the magnetic flux densities in regions 1 and 3 (out of the stator ferromagnetic regions) are negligible, current fields are Laplacian as follows [12], [13]:

$$\begin{aligned}
&\nabla^2 Jr1=0 \quad , \quad \nabla^2 Jr3=0\\
&\nabla^2 J\phi 1=0 \quad , \quad \nabla^2 J\phi 3=0\\
&r^2\frac{\partial^2 Jr1}{\partial r^2}+3r\frac{\partial Jr1}{\partial r}+(1-v'^2)Jr1=0\\
&r^2\frac{\partial^2 Jr3}{\partial r^2}+3r\frac{\partial Jr3}{\partial r}+(1-v'^2)Jr3=0\\
&r^2\frac{\partial^2 J\phi 1}{\partial r^2}+3r\frac{\partial J\phi 1}{\partial r}+(1-v'^2)J\phi 1=0\\
&r^2\frac{\partial^2 J\phi 3}{\partial r^2}+3r\frac{\partial J\phi 3}{\partial r}+(1-v'^2)J\phi 3=0.
\end{aligned} \tag{6}$$

The subscripts 1 and 3 refer to regions 1 and 3. The assumptions and simplifications made to obtain and solve the equations have completely been discussed in [13].

### B. Solutions

The solutions to (6) in regions 1 and 3 are

$$\begin{aligned}
Jr1&=C11\cdot r^{(-v'-1)}+C12\cdot r^{(v'-1)}\\
Jr3&=C31\cdot r^{(-v'-1)}+C32\cdot r^{(v'-1)}\\
J\phi 1&=j(C11\cdot r^{(-v'-1)}-C12\cdot r^{(v'-1)})\\
J\phi 3&=j(C31\cdot r^{(-v'-1)}-C32\cdot r^{(v'-1)})
\end{aligned} \tag{7}$$

where $C11, C12, C31$, and $C32$ are constants that can be obtained using the related boundary conditions.

Equation (5) is not easily solved, and in order to get a solution in the region under the stator [region (2)], two methods are presented.

*1) Method One:* The resultant field equations are solved analytically in Maple environment [15]. The particular solutions depend on the number of poles. Equation (5) has both a particular and a general answer. The particular solution depends on whether the number of pole pairs is odd or even, but the general solution remains unchanged.

If the number of pole pairs is odd, then

$$\begin{aligned}
Bz=&\,C21\cdot Besselk(v',j(jA)^{0.5}r)\\
&+C22\cdot Besselj(v',(jA)^{0.5}r)\\
&-B\cdot LommelS1(-1,v',(A)^{0.5}r)\\
j=\sqrt{-1},&\quad A=\left(v'\frac{2}{P}(1-s)-1\right)\cdot K\cdot\omega\\
B=\frac{\mu 0}{gt}v'\cdot r\cdot J'sm,&\quad J'sm=\frac{Jsm}{r}
\end{aligned} \tag{8}$$

where $LommelS1$, $Besselj$, and $Besselk$ are mathematical functions [15].

On the other hand, if the number of pole pairs is even, the solutions depend on harmonic order and the number of pole pairs. As an example, the fundamental component of $Bz$ for a four-pole motor is

$$\begin{aligned}
Bz=&\,C21\cdot Besselk(v',j(jA)^{0.5}r)\\
&+C22\cdot Besselj(v',(jA)^{0.5}r)-\frac{B}{Ar^2}.
\end{aligned} \tag{9}$$

The constants in (7), (8), and (9) are calculated from the boundary conditions in the region numbers (1)–(2) and (3). The boundary conditions are

$$\begin{aligned}
&Jr1(r=r0)=0\\
&Jr3(r=r3)=0\\
&Jr2(r=r1)=Jr1(r=r1)\\
&Jr2(r=r2)=Jr3(r=r2)\\
&J\phi 1(r=r1)=J\phi 2(r=r1)\\
&J\phi 2(r=r2)=J\phi 3(r=r2)
\end{aligned} \tag{10}$$

where $(r0, r3)$ and $(r1, r2)$ are respectively the inner and outer radii of the rotor and stator.

*2) Method Two:* To solve (5), the region under the stator [region (2)] is divided into many concentric circular areas as shown in Fig. 4. The coefficients ($r^2$ and $r$) in the first and second terms of (5) are assumed constant in each circular area. Hence, the equation is converted into a simple second-order equation. Now, the solution in each area is obtained as in the following:

$$\begin{aligned}
Bz(i)=&\frac{-jB}{jA-v'^2}+C21(i)\cdot\exp(\alpha_1(i)\cdot r)\\
&+C22(i)\cdot\exp(\alpha_2(i)\cdot r)\\
\alpha_1(i)=&\frac{-\frac{1}{r2'(i)}+\sqrt{\left(\frac{1}{r2'(i)}\right)^2-4\left(jA-\frac{v'^2}{r2'(i)^2}\right)}}{2}\\
\alpha_2(i)=&\frac{-\frac{1}{r2'(i)}-\sqrt{\left(\frac{1}{r2'(i)}\right)^2-4\left(jA-\frac{v'^2}{r2'(i)^2}\right)}}{2}\\
r2'(i)=&\,r1+\frac{(r2-r1)}{n}\cdot\frac{(2i-1)}{2}
\end{aligned} \tag{11}$$

where $n$ is the number of areas and $i$ is the area number.

The constants in (7) and (11) are calculated from the boundary conditions in the region numbers (1)–(2) and (3) as before. The boundary conditions are

$$\begin{aligned}
&Jr1|_{(r=r0)}=0\\
&Jr3|_{(r=r3)}=0\\
&Jr2(i=1)|_{(r=r1)}=Jr1|_{(r=r1)}\\
&J\phi 2(i=1)|_{(r=r1)}=J\phi 1|_{(r=r1)}\\
&\vdots\\
&Jr2(i)|_{(r=r2(i))}=Jr2(i+1)|_{(r=r2(i))}\\
&J\phi 2(i)|_{(r=r2(i))}=J\phi 2(i+1)|_{(r=r2(i))}\\
&\vdots
\end{aligned}$$

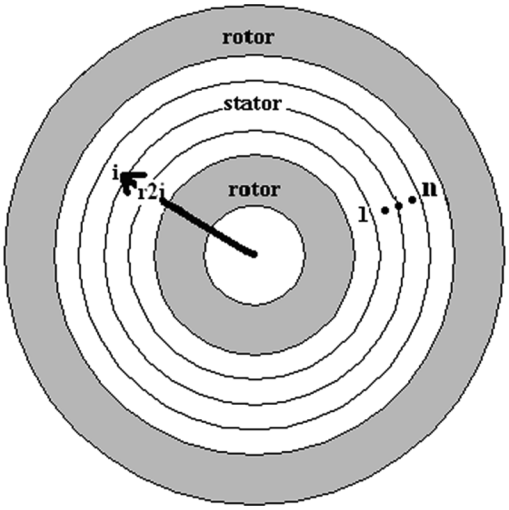


Fig. 4. Concentric circular areas of region (2).

$$
\begin{aligned}
&Jr2(i=n)\big|_{(r=r2)} = Jr3\big|_{(r=r2)}\\
&J\phi 2(i=n)\big|_{(r=r2)} = J\phi 3\big|_{(r=r2)}\\
&\vdots\\
&r2(i) = r1 + i\frac{(r2-r1)}{n}.
\end{aligned}
\tag{12}
$$

## III. Simulation

To evaluate the accuracy of the analytical model, an axial air gap induction motor with considerable space harmonics is selected. The motor has four poles, three phases, and 12 slots. Other specifications are in Table I. In order for the effects of harmonics to be high, one slot per pole per phase is chosen. The orders of the important existing harmonics are $1, -5, 7$, and $-11$, while the effects of the others are negligible. First, the solutions from method one is presented:

$$
\begin{aligned}
Bz,1 &= C21,1\cdot Besselk(2, j(jA)^{0.5}r)\\
&\quad + C22,1\cdot Besselj(2,(jA)^{0.5}r)\\
&\quad - BAr^{-2}\\
Bz,-5 &= C21,-5\cdot Besselk(10, j(jA)^{0.5}r)\\
&\quad + C22,-5\cdot Besselj(10,(jA)^{0.5}r)\\
&\quad - B(18579456\\
&\quad + 516096jAr^2 - 8064.A^2r^4 - 96jA^3r^6\\
&\quad + A^4r^8) * A^{-5}r^{-10}\\
Bz,7 &= C21,7\cdot Besselk(14, j(jA)^{0.5}r)\\
&\quad + C22,7\cdot Besselj(14,(jA)^{0.5}r)\\
&\quad - B(-3643696742\ 400\\
&\quad - 7007109120\ 0jAr^2729907200A^2r^4\\
&\quad + 5529600jA^3r^6 - 34560A^4r^8\\
&\quad - 192jA^5r^{10} + A^6r^{12}) * A^{-7}r^{-14}\\
Bz,-11 &= C21,-11\cdot Besselk(22, j(jA)^{0.5}r)\\
&\quad + C22,-11\cdot Besselj(22,(jA)^{0.5}r)\\
&\quad - B(-4870248707\ 1493088870\ 40000\\
&\quad - 5797915127\ 5587010560\ 000jAr^2\\
&\quad \times 3623696954\ 7241881600\ 0 * A^2r^4\\
&\quad \times 1589340769\ 615872000jA^3r^6\\
&\quad - 5518544338\ 944000A^4r^8\\
&\quad - 1623101276\ 1600jA^5r^{10}\\
&\quad + 42268262400A^6r^{12}\\
&\quad + 100638720jA^7r^{14}\\
&\quad - 224640A^8r^{16} - 480jA^9r^{18}\\
&\quad + \mathrm{A}^{10}\mathrm{r}^{20}) * A^{-11}r^{-22}.
\end{aligned}
$$

TABLE I
Design Data of the Machine (All Length Dimensions in Millimeters)

| Parameter | Value |
|---|---|
| $p$ | 2 |
| $q$ | 1 |
| $m$ | 3 |
| Stator inner diameter | 71 |
| Stator outer diameter | 128 |
| Rotor inner diameter(Al) | 15 |
| Rotor outer diameter(Al) | 184 |
| Rotor inner diameter(Fe) | 71 |
| Rotor outer diameter(Fe) | 128 |
| Rotor (Al) conductivity(S/m) | 3.278e7 |
| Relative Magnetic Permeability of Stator and Rotor Iron | 250 |
| Number of Stator Slots | 12 |
| Stator Height | 39 |
| Number of Turns per Coil | 290 |
| Stator Slot Opening | 3 |
| Stator Slot Width | 14 |
| Stator to Rotor Clearance | 1 |
| Rotor (Fe) Thickness | 25 |
| Rotor (Al) Thickness | 6.35 |
| Slot Height | 21 |
| Frequency | 50 |
| Current($I_l$) | 2 (A) |

As it can be seen, the solutions for the high harmonics are very complex and hard to solve.

The machine torque is obtained from the following equation:

$$
\begin{aligned}
\text{Torque} &= \pi\cdot r_{\text{mean}}\cdot(r2-r1)\\
&\quad\cdot \text{real}(Bz(r_{\text{mean}})\cdot\text{conjugate}(J'sm))\\
r_{\text{mean}} &= \frac{(r2+r1)}{2}.
\end{aligned}
\tag{13}
$$

To consider the effect of the magnetic flux of the winding overhangs and the related leakage fluxes, the width of stator core$(r2-r1)$ should be increased from 0.5 gt to 2 gt [10].

In using method two for simulation, the number $n = 21$ is found to give sufficient accuracy. The machine torque is obtained from the following equation:

$$
\begin{aligned}
\text{Torque} &= \sum_{i=1}^{n}\pi\cdot r2'(i)\\
&\quad\cdot\text{real}(Bz(r2'(i))\cdot\text{Conjugate}(J'sm)\cdot\Delta r\\
\Delta r &= \frac{r2-r1}{n}.
\end{aligned}
\tag{14}
$$

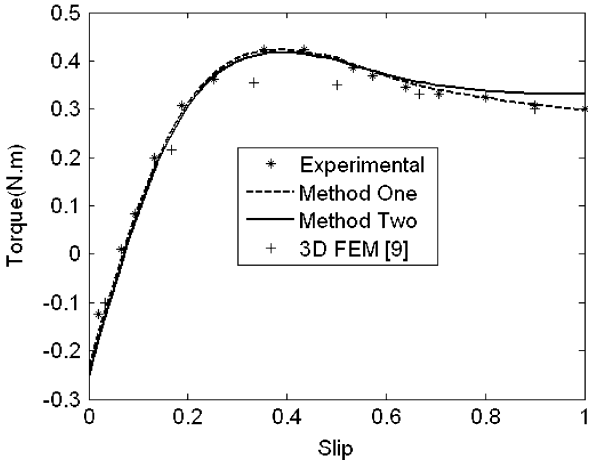


Fig. 5. Comparison of the predicted torque with the experimental one and 3-D FEM results [9].

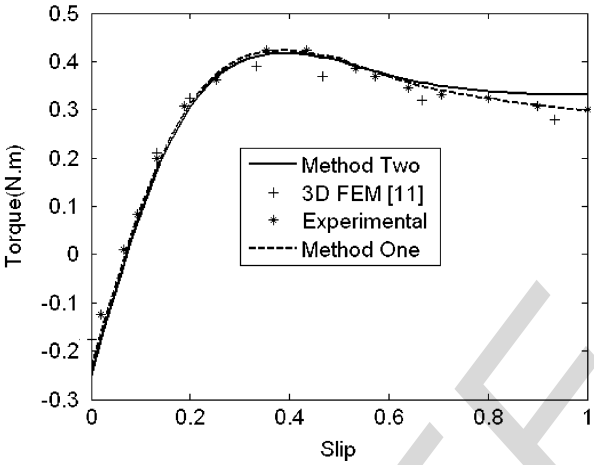


Fig. 6. Comparison of the predicted torque with the experimental one and 3-D FEM results [11].

Now, the results are compared with the experimental ones [9], [10] and depicted in Fig. 5. The calculated results coincide very well with the experimental ones. It is observed that the results of the presented method have higher accuracy in comparison with the 3-D FEM [9], [10]. The authors believe that one of the error sources of the 3-D FEM at low slips might be because of the chosen low mesh density (73 224 elements). Also in [11], the machine has been analyzed using 3-D FEM (882 561 elements). In [9], a stationary mesh has been used, and velocity and rotor motion effects have been directly employed in formulations. But in [11], a moving mesh has been applied. The results of [11] are compared with the obtained analytical ones in Fig. 6. The errors in [9] and [11] are considerable.

The obtained results of method one are better than method two, because an exact solution of field equations has been used.

The plots of computed magnetic flux density along with 3-D FEM results are shown in Figs. 7 and 8.

The 3-D FEM analysis has been carried out by OPERA-3D software with ELEKTRA module [16]. Comparison between analytical and 3-D FEM shows the accuracy of the proposed method in magnetic field calculations of axial air-gap in induction machines. The oscillations in 3-D FEM results of Fig. 8 are due to the teeth and slot effects.

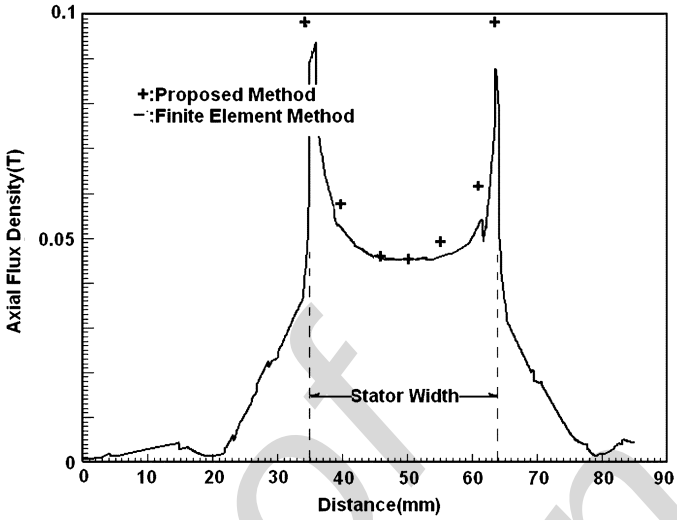


Fig. 7. Comparison between analytical and 3-D FEM in radial direction.

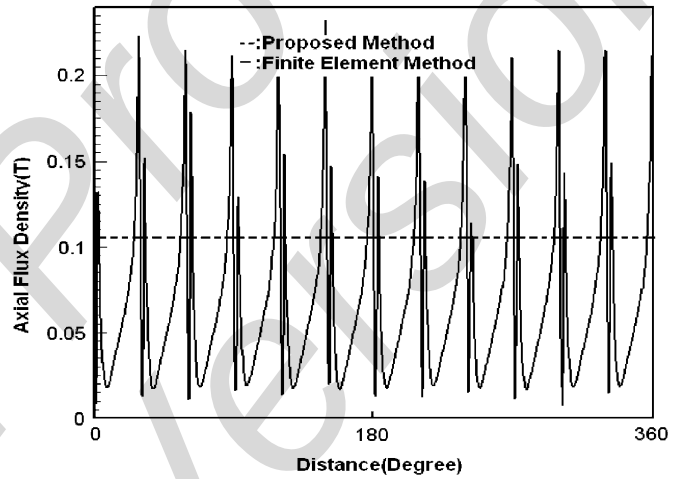


Fig. 8. Comparison between analytical and 3-D FEM in angular direction under the stator, in middle of the air gap and mean radius of the stator.

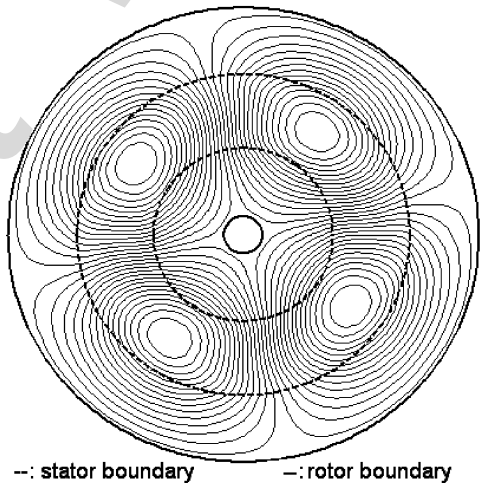


Fig. 9. Rotor current density distribution at zero speed.

The rotor current distribution at zero speed is shown in Fig. 9. One can deduce from the distribution that three-dimensional analysis is necessary for complete consideration of machine structure and exact prediction of its performance.

## IV. Conclusion

A direct solution of the field equations in cylindrical coordinates has been presented. The analytical method considers almost all dimensions of the machine. At low slips (normal operating region), the predicted points of both methods coincide with the experimental results with high accuracy. Hence, the proposed method has the ability of accurate performance prediction of axial air gap solid rotor induction machines. The presented approach helps designers to compute and evaluate performances of axial air gap induction machines with solid rotors in shorter time and with high accuracy.

**AUTHOR: The editor-in-chief requests that you please add two or more references to your paper citing recent *IEEE Transactions on Magnetics* articles (published in 2005-2007), to demonstrate that your paper is relevant to current interests of our audience. Please let me know if you are able to do this. Thank you. —Ed.**

## References

[1] S. Kubzdela and B. Weglinski, "Magnetodielectrics in induction motors with disk rotor," *IEEE Trans. Magn.*, vol. 24, no. 1, pp. 635–638, Jan. 1988.
[2] I. Boldea and S. A. Nasar, "Finite width, finite thickness and saturation effects in solid-rotor induction machines," *IEEE Trans. Power App. Syst.*, vol. 94, no. 5, pp. 1500–1507, Sep. 1975.
[3] H. May, "Analysis, performance and equivalent circuit of a disk-rotor induction machine," (in German) *ETZ A*, vol. 104, no. 10, pp. 574–577, 1973.
[4] H. Mosebach, "Analysis and characteristics of the disk-rotor induction machine," *Elect. Mach. Electromech.*, vol. 1, pp. 87–98, 1976.
[5] N. Esposito, A. Musolino, and B. Tellini, "Electromagnetic analysis of an induction motor with massive disk," *IEEE Trans. Magn.*, vol. 31, no. 3, pp. 2076–2079, May 1995.
[6] K. Ciosk, E. Gierczak, and E. Mendrela, "Analysis of electromagnetic field in a disk induction motor with double-sided stator and twin rotors using a 3-D reluctance network method," in *ICEM. 98*, Istanbul, Turkey, 1998, pp. 286–289.
[7] E. Mendrela, "Evaluation of magnetic field and forces in a single-phase induction disk motor with multi-layer rotor," *Arch. Elect. Eng.*, vol. XLIV, no. 2, pp. 263–273, 1996.
[8] A. I. Inkin and B. V. Litvinov, "The electromagnetic field in the gap of A.C. faceplate motors," *Elektrichestvo*, no. 11, pp. 67–71, 1974.
[9] D. Rodger, P. C. Coles, N. Allen, H. C. Lai, P. J. Leonard, and P. Roberts, "3D finite element model of a disc induction machine," in *IEE 8th Int. Conf. Electrical Machines and Drives (EMD97)*, 1997, pp. 148–149.
[10] D. Rodger, H. C. Lai, P. C. Coles, and R. J. Hill-Cottingham, "Modeling axial air gap induction machine," in *IEE Seminar Axial Air Gap Machines*, 2001, pp. 2/1–2/3.
[11] D. N. Dyck, B. Forghani, C. S. Brett, J. P. Webb, and D. A. Lowther, "A T-omega finite element method for arbitrary motion in 3D," presented at the Compumag 2005, Shenyang, China.
[12] S. A. Nasar and I. Boldea, *Linear Motion Electric Machines*. New York: Wiley, 1976.
[13] C. H. Lee and C. Y. Chin, "A theoretical analysis of linear induction motors," *IEEE Trans. Power App. Syst.*, vol. 98, no. 2, pp. 679–688, Mar. 1979.
[14] K. Oberretl, "Three-dimensional analysis of the linear motor," in *Transport Without Wheels*. London, U.K.: Elek Science, 1977, pp. 217–247.
[15] Maple ver. 7, Software User Guide. 2001.
[16] Pc-Opera ver.8.5, Software User Guide. 2002.

Manuscript received September 22, 2006; revised February 23, 2007. Corresponding author: M. Mirzaei (e-mail: mehranamirzaei@yahoo.com).

**Mehran Mirzaei** was born in Bandar Anzali, Iran, in 1977. He received the B.S. and M.S. degrees in electrical power engineering from Amirkabir University of Technology, Tehran, Iran, in 1999 and 2002, respectively.

Currently, he is with the EMTR Laboratory, Amirkabir University of Technology. His research interests are numerical and analytical analysis of electromagnetic fields, solid rotor and linear induction machines, and high-speed electric machines.

**Mojtaba Mirsalim** (SM'04) was born in Tehran, Iran, on February 14, 1956. He received the B.S. degree in EECS/NE and the M.S. degree in nuclear engineering from the University of California, Berkeley, in 1978 and 1980, respectively, and the Ph.D. degree in electrical engineering from Oregon State University, Corvallis, in 1986.

Since 1987, he has been at Amirkabir University of Technology, Tehran, where he has served five years as the Vice Chairman and more than seven years as the General Director in Charge of Academic Assessments, and currently is a Full Professor in the department of Electrical Engineering where he teaches courses and conducts research in energy conversion, electrical machine design, and hybrid vehicles, among others. His special fields of interest include the design, analysis, and optimization of electric machines, FEM, renewable energy and hybrid vehicles. He is the author of more than 90 international journal and conference papers and three books on electric machinery and FEM. He is the founder and at present, the director of the Electrical Machines & Transformers Research Laboratory (http://ele.aut.ac.ir/EMTRL/Homepage.htm).

**Seyed Ehsan Abdollahi** received the B.Sc. degree from Amirkabir University of Technology (Tehran Polytechnic), Tehran, Iran, with 1st rank of honor in 2002 and the M.S. degree from Iran University of Science & Technology, Tehran, in 2005, both in electrical engineering.

Currently, he is with the EMTR Laboratory, Amirkabir University of Technology. His current research interests are electric machine design and analysis including analytical and numerical methods and also modeling of microturbine generation systems.